Error analysis of a hexapod machine tool

J.A. Soons
Automated Production Technology Division
National Institute of Standards and Technology
Gaithersburg, MD 20899, U.S.A.
EMail: johannes.soons@nist.gov

Abstract

This paper describes the measurement and analysis of the quasi-static errors of a prototype hexapod milling machine at the National Institute of Standards and Technology (NIST). Emphasis is placed on a) the identification and definition of the parametric errors, b) the development of an analytical model to describe how these parametric errors affect errors in the position and orientation of the tool, c) identification of the most important parametric errors and their potential impact on performance, d) comparison of hexapod error characteristics to those of conventional machine tools, e) description of the techniques used to measure and estimate the hexapod errors, and f) application of the various concepts to model the geometrical and thermal errors of the NIST hexapod, including measurement results.

1 Introduction

Hexapods are mechanisms that provide controlled motion of a platform in all six degrees of freedom through a parallel arrangement of six kinematic chains or legs. Each leg contains only one actuated joint. In this paper consideration is given only to those machine tools where each leg has a linear actuator that is connected to the base and the platform through either two spherical or a spherical and a universal joint. These passive joints allow rotational movements such that each leg or strut effectively provides only one kinematic constraint between the platform and the base: that of distance.

Machine tools with the above configuration have a number of potential advantages over conventional machine tools [1,2]. These include high stiffness, low weight, low effective inertia of the moving components, and mechanical simplicity. Disadvantages include a complex workspace, a small orientation range, and, unless special measures are taken, low structural damping. Their accuracy is governed by different errors. Since each strut only realizes a distance, the roll, pitch, yaw, and straightness errors associated with

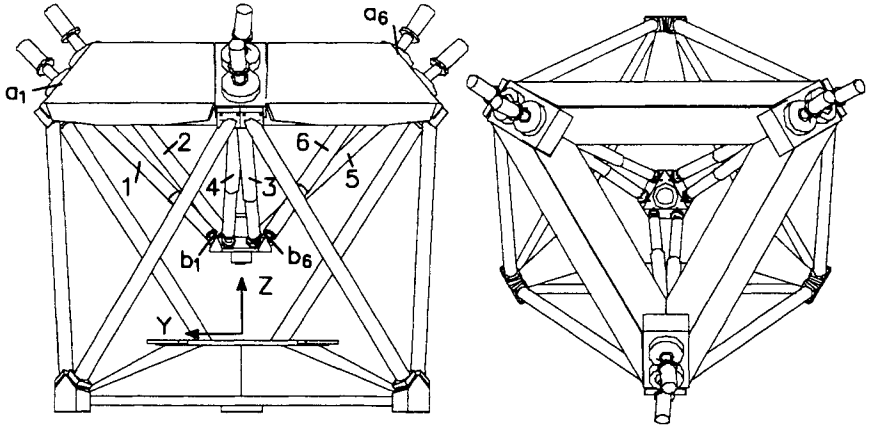

Figure 1: Front and top view of the prototype hexapod machine tool located at NIST

conventional machine axes are not important. However, a new class of errors is introduced. These errors stem from the positions of the platform and base joints, the accuracy of these joints, and the average length of the struts.

The prototype hexapod located at NIST is shown in Figure 1. The platform joints form a regular hexagon. The base joints are arranged in three pairs located on the corners of an equilateral triangle and are supported by an octahedral base frame. The characteristic radius through the platform joints is approximately seven times smaller than that through the base frame joints. The joints are ball and socket joints. The length of a strut is varied using a leadscrew-resolver arrangement with the nut connected to the lower telescoping part. Each strut has a stroke of 1400 mm and its average length equals 2860 mm.

2. The Kinematic Model

The kinematic model describes how errors in the actual geometry of the relevant machine components, i.e., parametric errors, cause errors in the position and orientation of the tool. In the derivation of the model, it is assumed that the errors are small and their effect on the propagation of other errors can be neglected. This assumption enables the use of rigid body kinematics to evaluate the error propagation without restricting the model to rigid structures. The result is a closed-form linear model completely defined by the nominal geometry of the hexapod. Though derived differently, it is similar to Ropponen's model [4] but differs from Wang's model which requires a forward solution [6].

Coordinate frames are attached to the base and to the platform. The latter frame is located on the spindle axis at the point where the tool length equals zero. The position and orientation of the platform frame as seen by the base frame are described by the vector coordinates $\mathbf{p}$ and the rotation matrix $\mathbf{R}$.

A strut, denoted by the subscript i, defines a distance l_i between a point $\mathbf{a}_i$ on the base and a point $\mathbf{b}_i$ on the platform. First, the error δl_i of this distance is related to the errors $\mathbf{e}$ and $\boldsymbol{\varepsilon}$ in the position and orientation of the platform, respectively. In this case, δl_i is approximated by the component of the movement of $\mathbf{b}_i$ in the nominal direction $\mathbf{n}_i$ of the strut:

$$\delta l_i = \mathbf{n}_i \cdot (\mathbf{e} + \boldsymbol{\varepsilon} \times \mathbf{R}\mathbf{b}'_i) = \mathbf{n}_i \cdot \mathbf{e} + (\mathbf{R}\mathbf{b}'_i \times \mathbf{n}_i) \cdot \boldsymbol{\varepsilon} \tag{1}$$

The prime symbol is used to indicate that the coordinates of point $\mathbf{b}_i$ are described in the platform frame. The error δl_i can also be expressed in the errors $\Delta\mathbf{a}_i$ and $\Delta\mathbf{b}_i$ in the position of the local centers of the joints, and error Δl_i in the strut length between these centers:

$$\delta l_i = \Delta l_i + \mathbf{n}_i \cdot (\Delta\mathbf{a}_i - \mathbf{R}\Delta\mathbf{b}'_i) \tag{2}$$

Combining equations (1) and (2) for all struts yields the kinematic error model:

$$\begin{bmatrix} \Delta l_1 + \mathbf{n}_1 \cdot (\Delta\mathbf{a}_1 - \mathbf{R}\Delta\mathbf{b}'_1) \\ \vdots \\ \Delta l_6 + \mathbf{n}_6 \cdot (\Delta\mathbf{a}_6 - \mathbf{R}\Delta\mathbf{b}'_6) \end{bmatrix} = \begin{bmatrix} \mathbf{n}_1^{\mathrm{T}} & (\mathbf{R}\mathbf{b}'_1 \times \mathbf{n}_1)^{\mathrm{T}} \\ \vdots & \vdots \\ \mathbf{n}_6^{\mathrm{T}} & (\mathbf{R}\mathbf{b}'_6 \times \mathbf{n}_6)^{\mathrm{T}} \end{bmatrix} \begin{bmatrix} \mathbf{e} \\ \boldsymbol{\varepsilon} \end{bmatrix} \tag{3}$$

$$\text{or: } \delta\mathbf{l} = \mathbf{J}\delta\mathbf{x}\text{, where } \delta\mathbf{x} = \begin{bmatrix} \mathbf{e} \\ \boldsymbol{\varepsilon} \end{bmatrix} \tag{4}$$

The errors $\mathbf{e}$ and $\boldsymbol{\varepsilon}$ in the location of the platform can be derived from the parametric errors $\Delta\mathbf{a}_i$, $\Delta\mathbf{b}'_i$, and Δl_i using the inverse of the Jacobian $\mathbf{J}$. This inverse exists in the stable part of the workspace, i.e., where the platform movement is constrained by the struts.

The kinematic model implies the following.

a) For each strut, a structural loop can be identified from spindle to platform to strut to base to workpiece and back to the spindle. Only the errors in this loop that act in the local direction of the strut are of importance. Therefore, straightness and angular errors of the linear actuator do not affect the hexapod accuracy nor does an offset of the strut in a spherical joint orthogonal to the strut direction.
b) In contrast to conventional machine tools, both the average and relative strut length error Δl_i are important.
c) The errors $\Delta\mathbf{a}_i$ and $\Delta\mathbf{b}'_i$ describe both errors in the position of a joint and errors of the joint. Only the joint error in the strut direction is important. Therefore a joint error can be modeled and measured as a single variable that is dependent on the orientation of the strut relative to the frame or base.

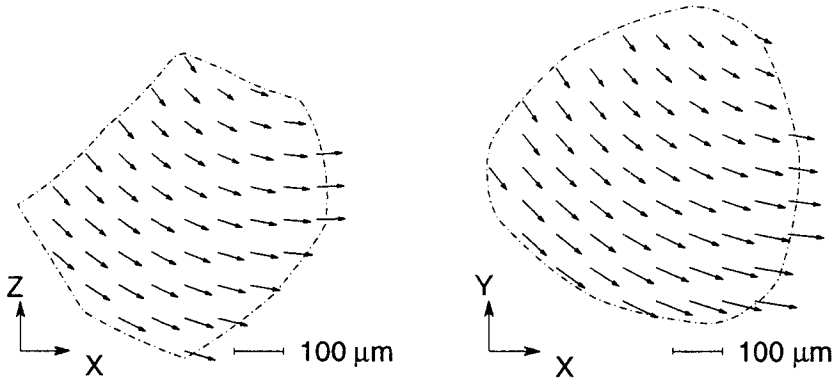

Figure 2: Error field in the central planes resulting from a constant error of 100 µm in the length of strut 3.

d) In general, the component of $\Delta\mathbf{a}_i$ that corresponds to a rigid body displacement of the base is not important, thus reducing the number of constant error parameters by six. However, the rigid body motion that varies in time due to thermal expansion of the base frame cannot be neglected.

e) The rigid body component of $\Delta\mathbf{b}_i'$ describes the errors in the position and orientation of the spindle. Since the roll error of the spindle is usually not important, the number of error parameters can be reduced by one. Spindle errors can be included in the model by either adding them to $\mathbf{e}'$ and $\boldsymbol{\varepsilon}'$ or by removing the respective rigid body movement from $\Delta\mathbf{b}_i'$.

f) The errors $\Delta\mathbf{a}_i$ and $\Delta\mathbf{b}_i'$ can be expressed in a local coordinate frame whose Z-axis points in the direction $\mathbf{m}_i$ of the strut when the joint is in its central position. For the base joints the respective coordinate transformation equals:

$$\Delta\mathbf{a}_i'' = \left[\frac{\mathbf{z}\times\mathbf{m}_i}{|\mathbf{z}\times\mathbf{m}_i|} \quad \frac{\mathbf{m}_i\times(\mathbf{z}\times\mathbf{m}_i)}{|\mathbf{z}\times\mathbf{m}_i|} \quad \mathbf{m}_i \right]^{\mathrm{T}} \Delta\mathbf{a}_i \tag{5}$$

The rows of the above matrix contain the direction vectors of the local coordinate frame. In practice, the orientation range of a strut is limited, typically in the order of ± 30°. Due to the limited angle β between the strut and $\mathbf{m}_i$, the contribution to the hexapod accuracy of the errors $a_{i,z}''$ and Δl_i are almost the same. The difference is difficult to estimate and only important at extreme platform orientations. The sensitivity of δl_i to $a_{i,x}''$ and $a_{i,y}''$ is limited by $\pm\sin\beta$. Similar arguments apply to the platform joints.

g) Because of the limited orientation range of the struts, a significant component of the error field resulting from Δl_i can be described by a rigid body displacement of the base (see Figure 2). Most of this component can be removed by subtracting the average strut length error $\underline{\Delta l}_i$ from Δl_i, adding it

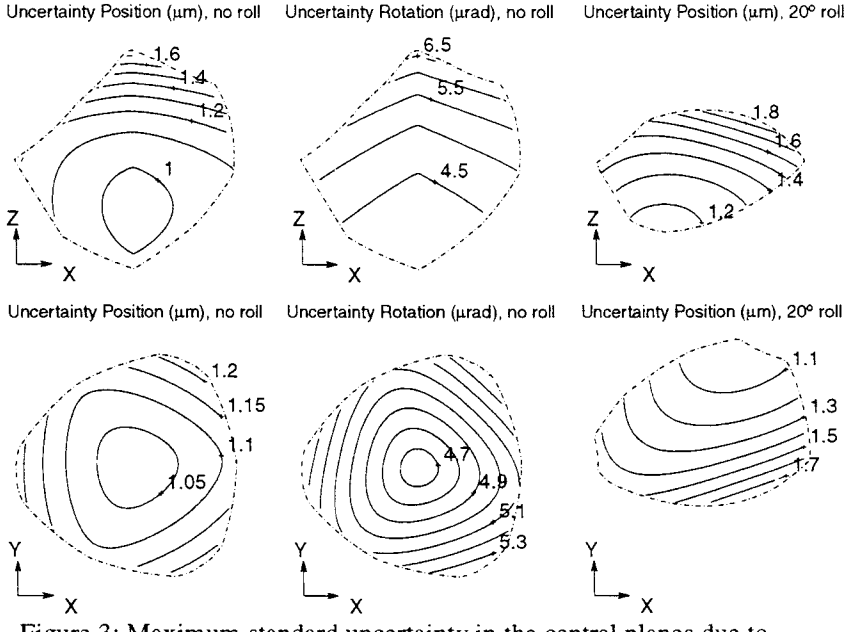

Figure 3: Maximum standard uncertainty in the central planes due to uncorrelated errors $\Delta \mathbf{l}$ with a variance of 1 μm^2.

to $a'_{i,z}$, introducing a new component of Δl_i equal to $(1-\cos\beta_i)\underline{\Delta l}_i$, and by removing the rigid body component of the modified errors $\Delta \mathbf{a}_i$.

h) Only the difference $\Delta \mathbf{a}_i - \mathbf{R}\Delta \mathbf{b}'_i$ is important. When the orientation of the platform is constant, the effect of $\Delta \mathbf{a}_i$ and $\Delta \mathbf{b}'_i$ cannot be separated nor is it important. In practice, because of the limited orientation range of the platform, the difference between $\Delta \mathbf{a}_i$ and $\Delta \mathbf{b}'_i$ is difficult to assess.

3. Sensitivity Analysis

Next an examination is made of the sensitivity of the hexapod errors to the various error parameters. The effects of the variation of the parametric errors are assessed by a variance analysis of the linear kinematic model. Figure 3 shows the standard uncertainty of the tool position along the longest axis of the uncertainty ellipsoid. The data are for uncorrelated length errors $\Delta \mathbf{l}$ having a variance of 1, and are calculated as the maximum eigenvalue of $(\mathbf{J}^{-1})_p \mathrm{Cov}(\Delta \mathbf{l})(\mathbf{J}^{-1})_p^T$. $(\mathbf{J}^{-1})_p$ represents the first three rows of the inverted Jacobian $\mathbf{J}$, modified for position errors at the tool tip for a tool length of 100 mm, and $\mathrm{Cov}(\Delta \mathbf{l})$ is the covariance matrix of $\Delta \mathbf{l}$.

In the center of the workspace, the errors in the X- and Y-directions are more sensitive to errors in $\Delta \mathbf{l}$ than are those in the Z-direction. Moving the platform up increases the sensitivity of the errors in the Z-direction to $\Delta \mathbf{l}$ and

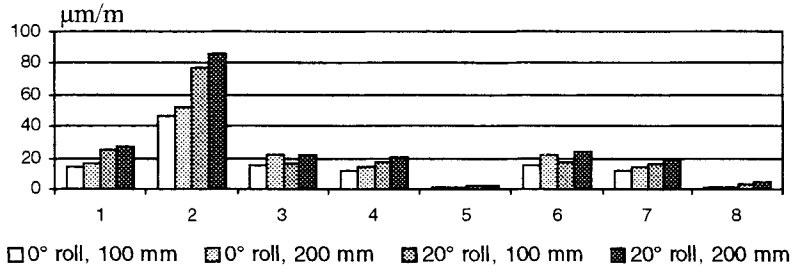

(1) $\Delta L_3 = 100\ \mu m$, (2) $\Delta L_3 = 100\ \mu m/m$,
(3) $\Delta a''_{3,x} = 100\ \mu m$, (4) $\Delta a''_{3,y} = 100\ \mu m$, (5) $\Delta a''_{3,z} = 100\ \mu m$ $\Delta L_3 = -100\ \mu m$,
(6) $\Delta b''_{3,x} = 100\ \mu m$, (7) $\Delta b''_{3,y} = 100\ \mu m$, (8) $\Delta b''_{3,z} = 100\ \mu m$ $\Delta L_3 = 100\ \mu m$

Figure 4: Relative length uncertainty (2σ) for different platform orientations, tool lengths, and parametric errors.

decreases it in the X- and Y-directions. Moving the platform away from the center and tilting it both increase the position uncertainty. The effect is more pronounced in the case of tilting. Angular errors were found more sensitive to errors in $\Delta \mathbf{l}$ than position errors. This is due to the small platform size. The result indicates that, because of the parallel nature of the hexapod, errors average rather than add. Accordingly, the error propagation is more favorable than that of conventional machine tools.

Analysis of variance tends to overstate the effects of constant or slowly varying parametric errors on hexapod errors. Therefore, the hexapod error sensitivity to a constant parametric error was obtained by calculating its effect on the errors in approximately 50 000 lengths distributed throughout the workspace. The results, expressed as the relative length error that encompasses $\pm 2\sigma$ of the simulated errors, are shown in Figure 4.

Another useful tool is that of parametric error shapes. A parametric error shape is the calculated error pattern at the target points of either a performance evaluation test or a machined part with all error parameters equal to zero except for one which is set equal to either 1 or some scaled value. Because both the error model and the tool path errors are linear with respect to the parameters, the error shape corresponding to an arbitrary set of parameter values can be calculated as the corresponding linear combination of the parametric error shapes. Figure 5 shows the parametric error shapes for a circular ballbar test with a horizontal platform orientation. Note the low sensitivity of the circularity errors to the parametric errors.

4. Error Measurement

Techniques to assess the parametric errors of a hexapod are examined below.

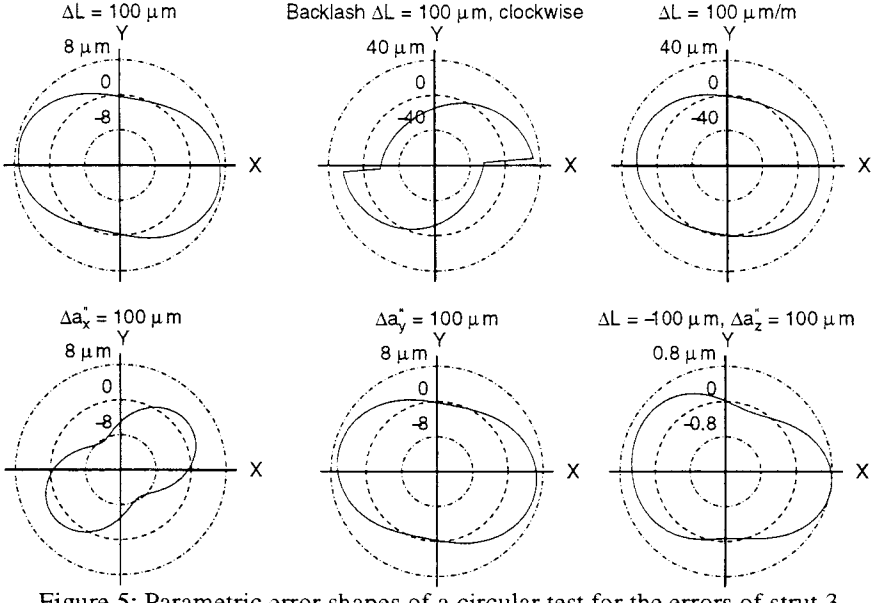

Figure 5: Parametric error shapes of a circular test for the errors of strut 3 (600 mm calibrated radius, lower XY-plane). Note the different scales.

4.1 Measurements on a Disassembled Machine

Measurements on disassembled machines can be performed to determine the dimensions of critical machine assemblies. These measurements are meaningful only when combined with kinematically repeatable assembly techniques [2].

4.2 Measurements of the Relative Motion of Machine Components

Tracking errors in the relative motion of hexapod components, e.g., the motion of a point on a strut relative to the base or the platform, yields powerful information on subsets of the parametric errors. Similar measurements can be performed to improve the accuracy of the hexapod during operation [7]. It should be noted that measurements between machine components other than the platform and the base are affected by errors, such as bending, straightness, and roll errors of the struts, that do not necessarily affect the hexapod accuracy.

4.3 Measurements of the Relative Motion of Platform and Workpiece

4.3.1 Measurement of all Position and Orientation Errors

Measurement of all errors in the position and orientation of the tool facilitates a separate analysis of the errors associated with each strut assembly. Some measurement techniques can be found in [3] and [8]. Equation 4 can be used to

compute the contribution of each strut assembly to the observed drift or repeatability of the tool at a specified location. However, error motion measured in space requires a different approach because it is measured relative to a reference whose position and orientation are unknown.

Measured errors $\mathbf{e}_m$ and $\boldsymbol{\varepsilon}_m$ in the platform location can be expressed as:

$$\begin{bmatrix} \mathbf{e}_m \\ \boldsymbol{\varepsilon}_m \end{bmatrix} = \begin{bmatrix} \mathbf{e} - \mathbf{e}_o - \boldsymbol{\alpha} \times \mathbf{p} \\ \boldsymbol{\varepsilon} - \boldsymbol{\varepsilon}_o \end{bmatrix} \tag{6}$$

where $\mathbf{e}_o$ and $\boldsymbol{\varepsilon}_o$ are the errors in platform location at the first point of the measurement and $\boldsymbol{\alpha}$ is the orientation of the reference. Usually $\mathbf{e}_o$, $\boldsymbol{\varepsilon}_o$, and $\boldsymbol{\alpha}$ are unknown, except for some setups where $\boldsymbol{\varepsilon}_o$ is defined by $\boldsymbol{\alpha}$. Inserting Equation (6) into Equation (3) yields:

$$\Delta l_i + \mathbf{n}_i \cdot \mathbf{m}_{i,k} = \mathbf{n}_i \cdot \mathbf{e}_m + (\mathbf{R}_k \mathbf{b}_i' \times \mathbf{n}_i) \cdot \boldsymbol{\varepsilon}_m \tag{7}$$

$$\text{where: } \mathbf{m}_{i,k} = \Delta \mathbf{a}_i - \mathbf{e}_o - \boldsymbol{\alpha} \times \mathbf{a}_i - \mathbf{R}_k (\Delta \mathbf{b}_i' + (\boldsymbol{\varepsilon}_o' - \boldsymbol{\alpha}') \times \mathbf{b}_i') \tag{8}$$

Assuming constant parametric errors, the error Δl_i and the vector $\mathbf{m}_{i,k}$ can be estimated from the measured errors $\mathbf{e}_m$ and $\boldsymbol{\varepsilon}_m$ during a path k with a constant platform orientation $\mathbf{R}_k$. Here the strut direction vectors $\mathbf{n}_i$ of the target points have to span a three dimensional space. Measurements along two orthogonal lines are sufficient. To improve the accuracy of the estimate or to account for variable parametric errors, more than four target points in a path may be used.

The estimation of $\Delta \mathbf{a}_i$ and $\Delta \mathbf{b}_i'$ requires measurements of a path with a new platform orientation $\mathbf{R}_k$, yielding a new vector $\mathbf{m}_{i,k}$ for each strut. Depending upon the setup, it may be necessary to introduce a new set of unknowns $\mathbf{e}_o$, $\boldsymbol{\varepsilon}_o$, and $\boldsymbol{\alpha}$. On the other hand, each setup yields 6×3 data points corresponding to the vectors $\mathbf{m}_{i,k}$, thus effectively providing nine new values. The number of unknowns in $\Delta \mathbf{a}_i$ and $\Delta \mathbf{b}_i'$ that can be estimated equals $6 \times (3+3) - 2 \times 6 = 24$, which implies that measurements are required at a minimum of three different platform orientations. Note that when a new set of unknowns $\mathbf{e}_o$, $\boldsymbol{\varepsilon}_o$, and $\boldsymbol{\alpha}$ is introduced for each new platform orientation, it is not possible to estimate the six components of $\Delta \mathbf{b}_i'$ that describe the location of the spindle in the platform frame. These errors can be assessed by rotating the tool around a single point, while measuring the errors in the realized position of that point (for two different lengths of the tool).

4.3.2 Arbitrary Performance Evaluation Tests

The error parameters can be simultaneously estimated such that some measure of the difference between the observed and predicted errors during a set of tests is minimized. The problem can be translated into the estimation of the linear

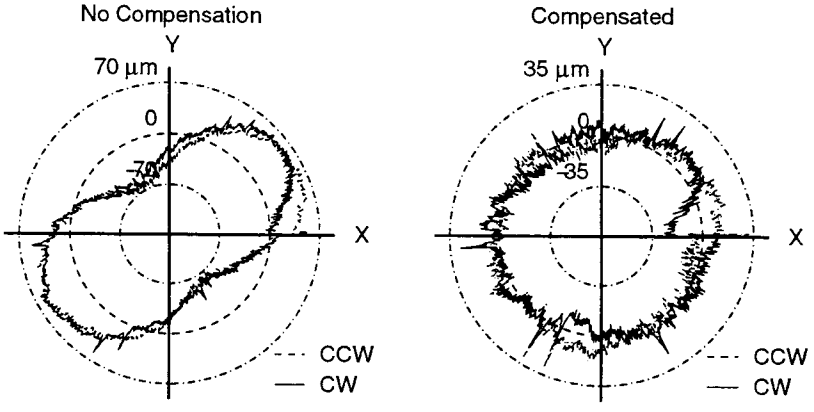

Figure 6: Measured errors during a circular test (lower plane, 600 mm uncalibrated radius). Note the 12 reversal peaks on the circle.

combination of parametric error shapes that approximates the observed errors. This is achieved by solving the equation $\mathbf{y} = \mathbf{X}\boldsymbol{\beta}$ by the least squares method. Here the vector $\mathbf{y}$ contains the observed errors during the test(s), the vector $\boldsymbol{\beta}$ contains the parameters to be estimated, and each column of the matrix $\mathbf{X}$ contains the parametric error shape(s) of a particular parameter. A significant parameter analysis is applied to improve the robustness of the estimated model. Computer-aided experimental design techniques [5] are being investigated to select a suitable set of tests that improves the condition of the estimation.

Figure 6 shows the results of an initial error compensation. The required error parameters were estimated using the results of circular ballbar tests in various locations and with several platform orientations and tool offsets, as well as tests where the tool is rotated around a single point while measuring the errors in the realized position of that point. The latter test is sensitive to errors in the position of the platform joints. To test the robustness of the estimation, a 600 mm ballbar was only used to verify the compensation.

Measurement techniques that yield information on a single parametric error or a limited set of parametric errors are under development. For the relative strut length error, an experimental setup was devised that uses laser-interferometric length measurements. The platform is moved along a line parallel to the strut whose length error is to be determined. If the programmed platform orientation is held constant during the movement, the strut and its spherical joints will not rotate. The tool offset is calculated such that the retroreflector is on the imaginary line that passes through the leadscrew. If the laser is aligned along the path of the retroreflector, the laser readout equals changes in the length of the strut, irrespective of the errors introduced by other joints and struts (as far as first-order effects are concerned).

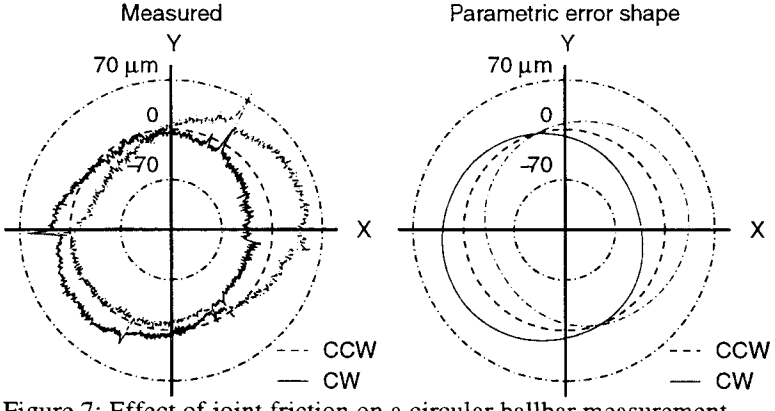

Figure 7: Effect of joint friction on a circular ballbar measurement. Solid lines indicate clockwise motion (300 mm calibrated radius, ballbar inclined 45°, platform rotated 15° around X)

5. Joint Friction

Joint friction causes bending of the struts resulting in a second-order error in their effective length. Far more important are the increased axial strut forces that cause elastic deformation that is dependent on the direction of motion. For horizontal platform movements, a major component of the resulting error motion is an angular error around a horizontal axis below the platform and orthogonal to the programmed path. As a result, the tool tip precedes the programmed motion when the tool length is large. On the hexapod located at NIST, angular reversal errors on the order of 35" were observed.

For ballbar measurements the effect is complex. When the platform is in a horizontal orientation, the identified angular error does not cause an error in horizontal circular contours. However, on a tilted platform the tool has an Abbe offset in the horizontal plane. This offset results in a position error in the Z-direction that changes direction when the motion is reversed. This position error acts in a sensitive direction when a horizontal circle is measured with the ballbar inclined relative to the plane of the circle (see Figure 7).

The following simplified procedure is used to calculate the effect of joint friction: (1) at each point along the tool path, the axis around which a strut is rotating is determined, (2) a constant friction moment around the identified axis of rotation is applied at each joint, (3) the resulting force and moment that each strut applies to the platform are calculated, (4) the force and moment that have to be applied to the platform to counteract the friction forces are calculated, and (5) the necessary change in the axial force of each strut [1] and the resulting length error are determined. The calculated scaled parametric error shape when all joints have an equal friction moment is shown in Figure 7. The estimation of

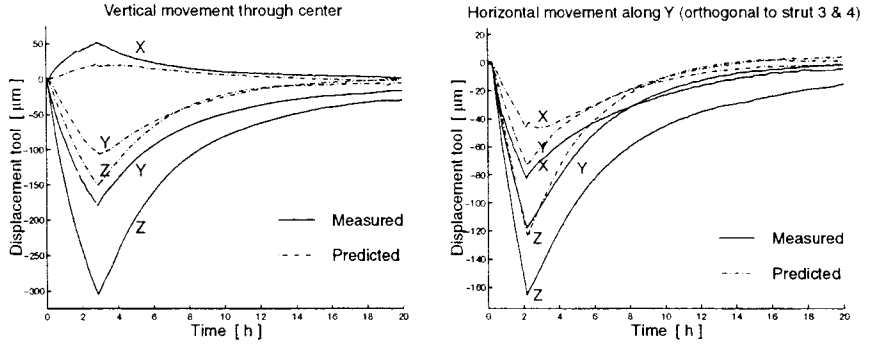

Figure 8: Measured position drift at a stationary position (lower plane, −400 mm from the center in Y-direction). Between measurements, the machine is moved with a feedrate of 6000 mm/min.

the friction moments of individual joints using the parametric error shape technique of Section 4.3.2 will be investigated.

6. Thermal errors

In the prototype hexapod at NIST, the major source of thermal errors is the thermal expansion of the struts due to the heat generated by friction in the telescope and the ballscrew drive. The struts are long and have no temperature invariant closed-loop metrology system. Temperature elevations resulting from the spindle are mainly confined to the platform and the lower part of the struts. No significant temperature elevation due to joint rotation has been observed.

A thermal error model was developed. The model is analytical and assumes a stress-free thermal expansion of the structural loop elements (i.e., outer frame, struts, and platform). Temperature elevations were measured using 34 thermocouples, located mainly on the struts. The observed and predicted drift of the tool due to various motion patterns of the platform are shown in Figure 8. Only a fraction of the observed drift is predicted because of difficulties in the determination of the effective temperature distribution of the leadscrew using sensors on the outer strut surface. Improved temperature measurement techniques and laser-interferometric measurements of strut expansion after different movement patterns are studied to improve the model.

Conclusions

The errors of a hexapod in an unloaded reference state, i.e., the geometric errors, are determined by 35 constant parameters and 18 functions. The relevant errors in the position of the base and platform joints are described by 12 and 17 constants, respectively. Six constant parameters describe the errors in the average strut lengths. The errors in the relative strut lengths are described by six

functions. Finally, 12 functions are required to describe the variation of the relevant joint errors due to changes in the strut orientation.

On the prototype hexapod at NIST, the errors in the relative strut length could be measured individually. The constant error parameters that significantly affect the hexapod accuracy could be estimated simultaneously by using metrology tools developed for the performance evaluation of conventional machine tools. However, there is no straightforward relationship between the results of conventional performance evaluation tests and the parametric errors. Further research is needed to identify more optimized error assessment procedures, including those focused on subsets of the error parameters.

The measurements on the prototype indicate the need for closed-loop thermally invariant metrology that addresses the length of the total strut, low-friction high-stiffness joints, and a higher structural damping.

References

1. Arai, T., et al., Design, analysis, and construction of a prototype parallel link manipulator, *IEEE International Workshop on Intelligent Robots and Systems*, pp. 205-212, 1990.
2. Bailey, P., The merits of hexapods for robotic applications, *IEE Colloquium – Next Steps for Industrial Robotics*, IEE Computing and Control Division C15 (Robotics), London, United Kingdom, 1994
3. Hocken, R.J., Ed., Machine tool accuracy, Volume 5 of *Technology of machine tools: A Survey of the State of the Art by the Machine Tool Task Force,* University of California, Livermore, CA, 1980.
4. Ropponen, T., and Arai, T., Accuracy analysis of a modified Stewart platform manipulator, *Proceedings of the IEEE International Conference on Robotics and Automation*, pp. 521 – 525, 1995.
5. Soons, J.A., and Schellekens, P.H., On the calibration of multi-axis machines using distance measurements, *Proceedings International Symposium on Metrology and Quality Control in Production*, pp. 321-340, 1992
6. Wang, J., and Masory, O., On the accuracy of a Stewart platform – Part I The effect of manufacturing tolerances," *Proceedings of the IEEE International Conference on Robotics and Automation*, pp. 114-120, 1993
7. Zhuang, H., Liu, L., Self-calibration of a class of parallel manipulators, *Proceedings of the IEEE International Conference on Robotics and Automation*, pp. 994 – 999, 1996.
8. Ziegert, J.C., and Mize, C.D., Laser ball-bar: A new instrument for machine tool metrology, *Precision Engineering*, 16, pp. 259-267, 1994.